Twists to the spin structure of the Ln9-diabolo motif exemplified in two {Zn2Ln2}[Ln9]{Zn2} coordination clusters

Article (Accepted Version)

Twists to the spin structure of the Ln_9-diabolo motif exemplified in two $\{Zn_2Ln_2\}[Ln_9]\{Zn_2\}$ coordination clusters

Kieran Griffiths,[†] Irina A. Kühne,[‡±] Graham J. Tizzard,[§] Simon J. Coles,[§] George E. Kostakis,[†] and Annie K. Powell*[‡⊥]*

† Department of Chemistry, School of Life Sciences, University of Sussex, Brighton BN1 9QJ, UK.

‡ Institut für Anorganische Chemie, Karlsruher Institut für Technologie (KIT), Engesserstr. 15, 76131 Karlsruhe, Germany

§UK National Crystallographic Service, Chemistry, University of Southampton, Southampton, SO1 71BJ, United Kingdom

⊥ Institut für Nanotechnologie, Karlsruher Institut für Technologie (KIT), Hermann-von-Helmholtz-Platz 1, 76344 Eggenstein-Leopoldshafen, Germany

± Current address : University College Dublin, School of Chemistry, Science Centre Belfield, Dublin 4, Ireland

ABSTRACT

Two pentadecanuclear Zn_4Ln_{11} [with Ln = Gd(**1**) or Dy(**2**)] coordination clusters, best formulated as $\{Zn_2Ln_2\}[Ln_9]\{Zn_2\}$, are presented. The central $\{Ln_9\}$ diabolo core has a $\{Zn_2Ln_2\}$ handle motif pulling at two outer Ln ions of the central core via two {ZnLn} units, which also invest the system with C_2 point symmetry. The resulting cluster motif is supported on two Zn "feet", corresponding to the $\{Zn_2\}$ unit in the formula. A thorough investigation of the magnetic properties in the light of the properties of previously reported $\{Ln_9\}$ diabolo compounds was undertaken. Up to now, the spin structure of such diabolo motifs usually proves ambiguous. Our magnetic studies show that the

orientation of the central spin in the $\{Gd_9\}$ diabolo plays a decisive role. In stabilizing the core by attachment of the $\{Zn\}^{2+}$ "feet" and using the C_2 symmetry related $\{ZnGd\}^{5+}$ handles to influence the spin direction of the central Gd of the $\{Gd_9\}$ diabolo we can understand why the "naked" $\{Gd_9\}$ diabolo shows ambiguous spin structure. This then allowed us to elucidate the single molecule magnetic (SMM) properties of the Dy based compound **2** through disentangling the magnetic properties of the isostructural Gd based compound **1**.

Introduction

The possibility to combine the properties of 3d and 4f elements within one molecule has received tremendous attention, resulting in reports on numerous 3d/4f heterometallic coordination clusters (CCs) showcasing aesthetically pleasing structures.[1] The idea behind creating 3d/4f CCs is to provide new systems with enhanced catalytic parameters,[2] steering of relaxation processes in 3d/4f Single Molecule Magnets (SMMs)[3–7] as well as exotic electronic and magnetic structures. This has been most recently exemplified in the [$Fe_{10}Gd_{10}$] system which stabilizes a maximal S = 60 ground spin whilst sitting poised next to a Quantum Critical Point in terms of its energy landscape.[8]

A relatively frequently occurring motif in coordination cluster chemistry is the nonanuclear "diabolo" arrangement of metal ions which is described as **4,8M9-1** (Figure 1) using the graph theory based topological analysis for discrete CCs,[9] applicable to known 3d[10,11] and 4f[12–14] based compounds. This motif can be envisaged as the vertex sharing fusion of two square-based pyramid units and for both motifs and the spin structures have always proved to be often intriguing although also ambiguous.[12,14–18]

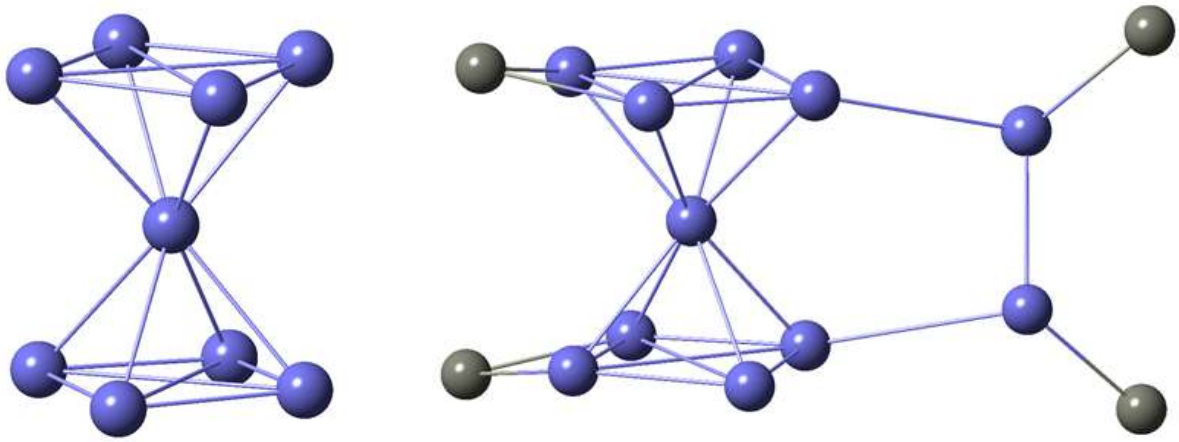

Figure 1. (left) The diabolo shaped **4,8M9-1** motif; (right) the decorated **1,2,3,4,5,5,5,8M15-1** motif observed in **1** and **2** illustrating the handles and feet stabilizing the structure.

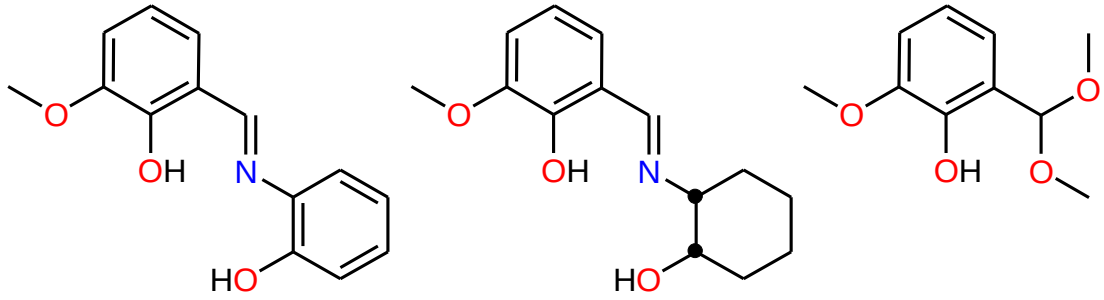

H_2L1 H_2L2 HL3

Scheme 1. The protonated form of the organic ligand H_2L1 (left), used in previous studies, H_2L2 (middle) used in this study; in situ formed ligand HL3 (right) observed in **1** and **2**.

So far no one has succeeded in combining the diabolo motif into a 3d/4f system. We have previously demonstrated that it is possible to combine Zn^{II} and 4f ions using the ligand H_2L1 (Scheme 1, left) to give a series of "butterfly" $Zn^{II}_2Ln^{III}_2$ CCs showing excellent catalytic efficiency.[19] However, our use of H_2L2 (Scheme 1, center) in a reaction aimed at producing a chiral Zn_2Ln_2 butterfly, resulted instead in an unprecedented transformation of some of the H_2L2 ligand to the achiral HL3 ligand (Scheme 1, right) accompanied by the stabilization of one of the largest Zn/4f CC so far reported with nuclearity 15.[20–22]

The structure forms around the well-known Ln_9 CC "diabolo" motif which is decorated with a $\{ZnLn\}_2$ unit above and two Zn^{II} ions below which are arranged such that the molecule has C_2 symmetry and is thus chiral. An analysis of the magnetic properties of the system and the influence of the C_2 symmetry on the overall spin structure helps shed light on the ambiguous magnetic properties which are observed in all CCs with a Ln_9 diabolo motif reported so far. To explain this further, we briefly summarize the results from the literature to date.

We can thereby unravel the spin structure ambiguity observed in all the previously reported pure Ln_9 diabolos. The observation that the inherent ambiguity of the diabolo spin structure is substantiated by the fact that in this case the system does not correspond to the S = 77/2 Brillouin function expected for the case where all the spins are parallel for the compound containing 11 isotropic Gd^{III} ions.

EXPERIMENTAL SECTION

Materials. Chemicals (reagent grade) were purchased from Sigma Aldrich and Alfa Aesar. All experiments were performed under aerobic conditions using materials and solvents as received.

Instrumentation. IR spectra were recorded over the range of 4000-650 cm^{-1} on a Perkin Elmer Spectrum One FT-IR spectrometer fitted with a UATR polarization accessory. TGA analysis was performed on a TA Instruments Q-50 model (TA, Surrey, UK) under nitrogen and at a scan rate of 10 °C/min (University of Sussex). Elemental Analysis measurements were performed at London Metropolitan University.

Magnetic studies. The magnetic susceptibility measurements were obtained using a Quantum Design SQUID magnetometer MPMS-XL operating between 1.8 and 300 K. DC measurements were performed on a polycrystalline sample of 11.9 mg (**1**) and 4.9 mg (**2**). The sample was wrapped in a polyethylene membrane and subjected to fields in a range from 0 to 7 T. Diamagnetic corrections were applied to correct for contribution from the sample holder, and the inherent diamagnetism of the sample was estimated with the use of Pascal's constants. AC measurements were carried out in with frequencies between 1 to 1500 Hz.

Preparation of compounds 1-2. *o*-Vanillin (0.2mmol) and (1*S*,2*S*)-*trans*-2-aminocyclohexanol hydrochloride (0.2mmol) were stirred in MeOH (20mL) for 2h to form a clear light-yellow solution. $LnCl_3.5H_2O$ (0.1mmol) and $Zn(NO_3)_2.6H_2O$ (0.2mmol, 56mg) were subsequently added along with Et_3N (0.45mmol, 61µL). The solution was stirred for a further 1h after which the solution had become colorless. The solution was filtered and the filtrate left for slow evaporation in air. Colorless needle shaped crystals were collected after 13 and 27 days for **1** and **2**, respectively. The yield based on Ln^{III} is 15% (**1**) and 21% (**2**). Elemental analysis of dried samples CHN $C_{80}H_{135}Cl_4Gd_{11}N_{10}O_{70}Zn_4$ (**1**) (expected) C-21.39%, H-3.03, N-3.12% (observed) C-21.52%, H-2.88%, N-3.00%, $C_{80}H_{135}Cl_4Dy_{11}N_{10}O_{70}Zn_4$ (**2**) (expected) C-21.08%, H-2.99, N-3.07% (observed) C-20.95%, H-3.27%, N-3.11%;

X-ray Crystallography. Data for **1** and **2** were collected at the National Crystallography Service, University of Southampton[23] on a Rigaku FRE+ diffractometer equipped with a HG Saturn 724+ CCD detector under a flow of nitrogen gas at 100(2) K, processed with CrysAlisPro and solved by intrinsic phasing methods with SHELXT.[24] Both crystal structures were then refined on Fo^2 by full-matrix least-squares refinements using SHELXL.[24] All non-H atoms were refined with anisotropic thermal parameters, and H-atoms were introduced at calculated positions and allowed to ride on their carrier atoms. Geometric/crystallographic calculations were performed using PLATON,[25] Olex2,[26] and WINGX[27] packages; graphics were prepared with Crystal Maker.[28] CCDC 1551722 (**1**) and 1551723 (**2**)

RESULTS AND DISCUSSION

Synthesis and Crystal description. Reaction of *o*-vanillin, (1*S*,2*S*)-*trans*-2-aminocyclohexanol hydrochloride, $LnCl_3{\cdot}xH_2O$, $Zn(NO_3)_2.6H_2O$ and Et_3N leads to the formation of the two new pentadecanuclear 3d-4f CCs. The compounds of formula $[Zn^{II}_4Ln^{III}_{11}(\mu_4\text{-}O)_2(\mu_3\text{-}OH)_8(\mu_2\text{-}OH)_2(NO_3)_8Cl_4(HL2)_2(L3)_4(\mu_2\text{-}MeO)_7(\mu_3\text{-}MeO)_2(MeOH)_2(H_2O)_2]$ x(MeOH) where Ln = Gd for **1** and Dy for **2**, provide a number of novel features: i) The coordination chemistry of H_2L2 has received little attention and has never been used in 3d or 4f or 3d/4f chemistry.[29] ii) the *o*-vanillin moiety gives an unseen chemical transformation yielding HL3, iii) the topology of the pentadecanuclear compounds has never been observed before.

Compounds **1** and **2** crystallize in the monoclinic space group C2/c with $Z = 4$ and are isoskeletal. The structure of **1** will be exemplarily described and is shown in Figure 2.

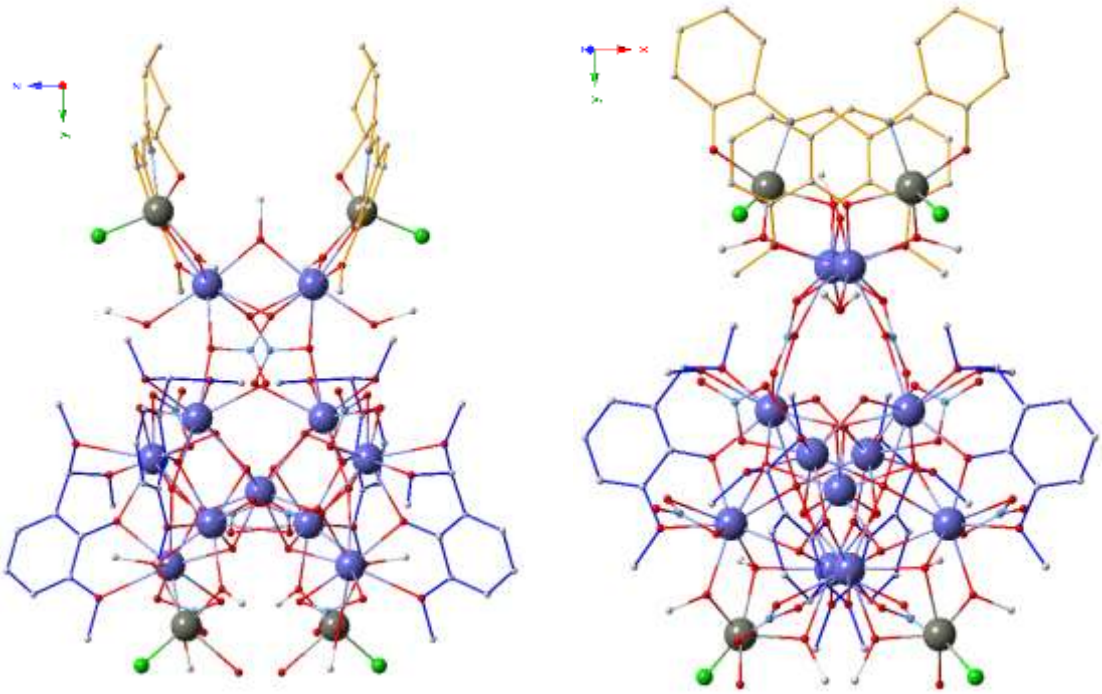

Figure 2. The molecular structure of compound **1** along *a* (left) and *c* (right) axis. The H_1L2^- moieties are highlighted in yellow, whereas the $L3^-$ moieties are highlighted in blue. Color code Ln (mauve), Zn (grey), C (light grey), N (light blue), O (red), Cl (light green).

The pentadecanuclear core consists of two units; a trianionic undecanuclear $[Zn^{II}_2Ln^{III}_9(\mu_4\text{-}O)_2(\mu_3\text{-}OH)_8(\mu_2\text{-}OH)_2(NO_3)_8Cl_4(L3)_4(\mu_2\text{-}MeO)_4(\mu_3\text{-}MeO)_2(H_2O)_2]^{3-}$ "body" unit (Figure 3, upper) and a tricationic tetranuclear $[ZnLn_2Zn(HL2)_2(\mu_2\text{-}MeO)_3Cl_2(MeOH)_2]^{3+}$ "handlebar" unit (Figure 3, lower). Within the Zn_2Ln_9 part, the nonanuclear lanthanide unit is held together by two μ_4- O^{2-} (O29), eight μ_3-OH^- (O25, O26, O27, O28 and their symmetry-related counterparts), two μ_2-OH^- molecules (O30) and four in situ formed *o*-vanillin derivatives $L3^-$ (Scheme 1). This nonanuclear motif is often referred to as "diabolo" shaped and has been identified in several compounds.[14,16,30–33] The diabolo description derives from the similarity to the topology of a double spinning top which a player performs tricks with using a two-handled rope. In the compound we describe here, the hands and rope are provided by the "handlebar unit", corresponding to Zn2 and Ln6 and their symmetry equivalents, respectively, the diabolo is provided by the Ln_9 core, where Ln2, Ln3, Ln4 and Ln5 (and their symmetry

related counterparts) form two square planes arranged as a square antiprism with Ln1 in the middle. The "feet" of the player correspond to the lower two Zn2 and Zn2' ions (see Figure 3).

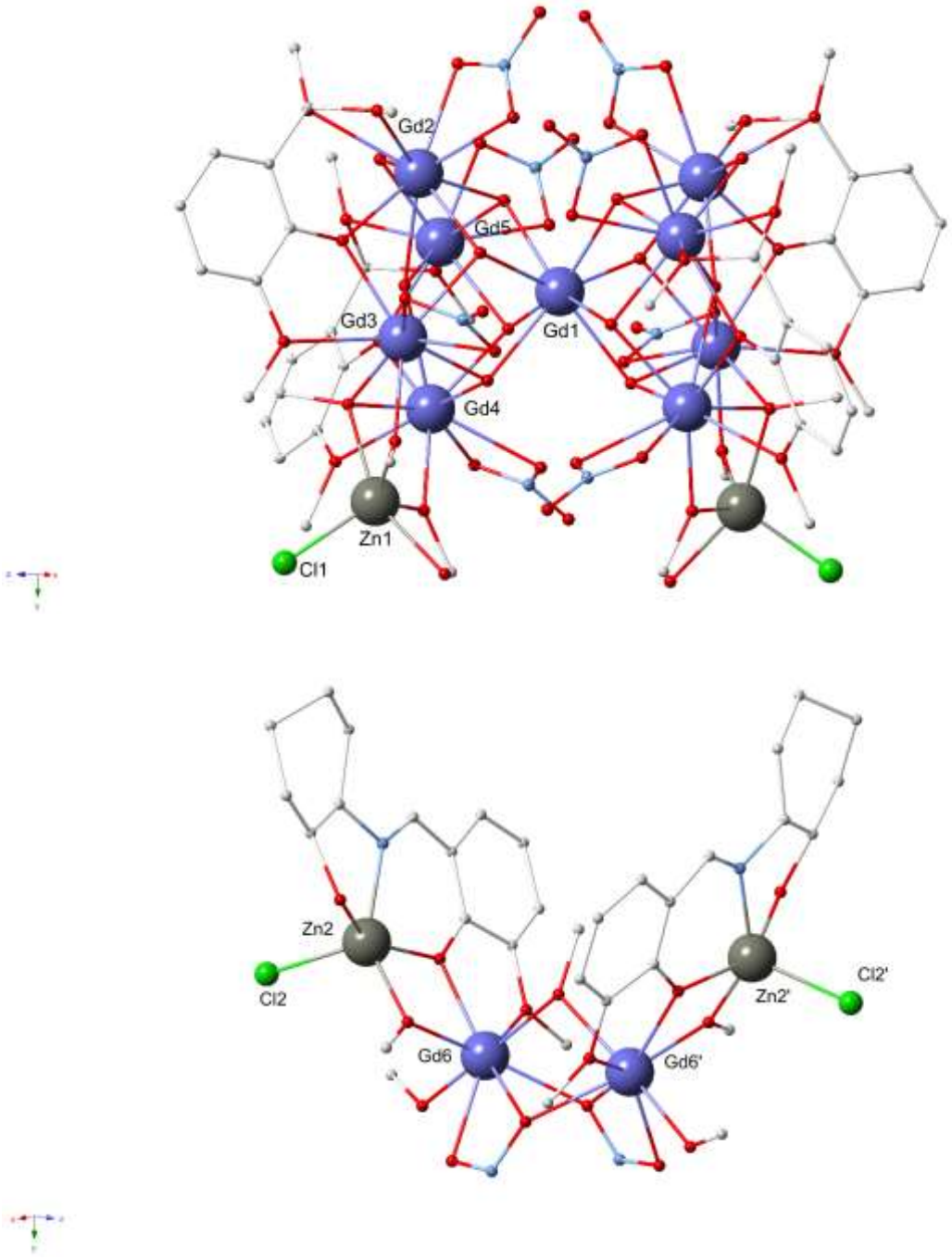

Figure 3. The undecanuclear $[Zn^{II}_2Ln^{III}_9(\mu_4\text{-}O)_2(\mu_3\text{-}OH)_8(\mu_2\text{-}OH)_2(NO_3)_8Cl_2(L3)_4(\mu_2\text{-}MeO)_4(\mu_3\text{-}MeO)_2(H_2O)_2]^{3-}$ "body" unit (upper) and tetranuclear $[ZnLn_2Zn(HL2)_2(\mu_2\text{-}MeO)_3Cl_2(MeOH)_2]^{3+}$ "handlebar" unit (lower). Color code Ln (mauve), Zn (grey), C (light grey), N (light blue), O (red), Cl (light green).

The lanthanide ions within the complex show different coordination environments, and while Gd1 and Gd6 are 8-coordinated the remaining ions, such as Gd2, Gd3, Gd4 and Gd5 are 9-coordinated. In order to describe the geometries of the metal ions within the structures, since that has an important effect on the magnetic behavior,[34–36] each metal center was analyzed using the SHAPE program.[37] The continuous shape analysis measures the deviation (in %) from an idealized polyhedron, with zero being ideal. This analysis (Table S2, ESI) reveals that the central Ln1 ion, which is the metal ion located in the center of the diabolo, has an almost perfect square antiprismatic geometry (0.33% deviation from SAPR-8). The two Ln6 metal ions, which are part of the tetranuclear handle bar and are 8-coordinated as well, are more distorted in the coordination environment and the smallest deviation was found to be biaugmented trigonal prismatic (BTPR-8 in Table S3) with a deviation of 3.86%. On the other hand, the 9-coordinate Ln^{III} ions are close to a spherical capped square antiprism (CSAPR-9 in Table S2), with a deviation between 1.41-1.87% from the perfect geometry, although in case of Gd3, the surrounding atoms are closer to a muffin topology with a deviation of 1.34%. For further information see ESI.

The *o*-vanillin derivative (L3, Scheme 1) and the in situ formed Schiff base ligand HL2 (Scheme 1) both bridge two metal centers (Scheme S1). The nonanuclear Ln_9 core is connected by two triply bridging methoxido units (O3) bridging Gd3, Gd4 to Zn1 and the symmetry equivalents, thus forming the undecanuclear core. Attachment of Zn1 to the Gd_9 unit is further supported by two doubly bridging methoxido moieties (O2 and O4). Gd2, Gd3 and Gd4 are chelated by a nitrate moiety, whereas Gd5, Gd6 and Gd6' are linked by another tridentate nitrate group thus providing attachment to the main core and the tetranuclear unit. Gd6 and Gd6' are bridged by a methoxido moiety (O32), whereas Gd6 is linked to Zn2 by doubly bridging methoxido (O33) and phenoxido (O35) units. Both Zn metal centers are 5-coordinate. Zn1 has a coordination geometry between square-based pyramidal and trigonal bipyramidal with a trigonality index $\tau = 0.46$, whereas Zn2 possesses an almost ideal square pyramidal geometry (trigonality index $\tau = 0.06$).[38]

Topological aspects. The decorated-metallic core of compounds **1** and **2** can be enumerated as **1,2,3,4,5,5,5,8M15-1** (Figure 1)[9] and has never been seen in polynuclear coordination chemistry before. From the automatic graph based search of TOPOS a comparison of the topology of the present compounds with previously reported compounds containing the diabolo motif (**4,8M9-1** graph)[14,16,30–33] provides very interesting structural data which has not been identified previously in any structural description which are summarized in Table 1.

A) In both **1** and **2**, the two Ln_4 planes are not parallel to each other. For **1** they are tilted at an angle of 0.888° and for **2** at 1.157°. These values lie between those reported for previous examples, which range from 0.290°–0.535°[31–33] for the nearly co-parallel examples to the significantly tilted Dy_9 example reported by Tang et al. where the angle is 1.809°.[12]

B) The two μ_4-O^{2-} bridges are placed 0.382Å (in **1**) and 0.393 Å (in **2**) above the Ln_4 plane; these values are significantly higher than those previously reported ranging from 0.147 Å to 0.325 Å.

C) The nonanuclear core in **1** and **2** is tetra-anionic, while all previous reported compounds are singly positively or negatively charged (see Table 1). The observed structural features for the compounds reported here are probably directed by the attachment of the $ZnLn_2Zn$ handlebar unit to the nonanuclear core providing the twist to the structure.

To further identify the purity of these compounds, thermogravimetric analysis (N_2 atmosphere, Figure S1) of a dried sample for compound **1** shows that it is stable up to 250^{o}C. The final residue of the decomposition fits well to the corresponding $Zn_4Gd_{11}O_{20.5}$ oxide, calculated 51.62%, found 51.14%.

Table 1. Structural characteristic of reported compounds containing the diabolo (**4,8M9-1**) motif.

Compound	**Reference**	**Metal**	**Ln_9 charge core**	**Ln_4 plane CN**	**Ln central CN**	**Ln_4 planes angle**	**Ln_4 planes distance**	**Nuclearity**	**O distance from Ln_4 plane**	**Space Group**
Gd_{17}	[39]	Gd	Neutral	9	8	0	5.499	17	0.319	P4212
Dy_{17}	[39]	Dy	Neutral	9	8	0	5.482	17	0.325	P4212
Dy_9	[12]	Dy	1+	8	8	**1.809**	**5.772**	9	0.147	C2/c
Dy_9	[31]	Dy	1+	9	8	0.535	5.672	9	0.300	C2/c
Dy_9	[16]	Dy	1+	9	8	0	5.759	9	0.248	P4/n
Gd_9	[16]	Gd	1+	9	8	0	5.759	9	0.248	P4/n
Gd_9	[40]	Gd	1+	8	8	0	5.427	9	0.266	Pn-3n
Dy_9	[40]	Dy	1+	8	8	0	5.372	9	0.270	Pn-3n
Gd_9	[32]	Gd	1-	8	8	0.541	5.319	9	0.236	C2/c
Gd_9	[33]	Gd	1+	8	8	0.326	5.329	9	0.271	Pbcn
Dy_9	[32]	Dy	1-	8	8	0.29	5.238	9	0.236	C2/c
Zn_4Gd_{11} (**1**)	This work	Gd	**4-**	9	8	0.888	5.559	15	**0.382**	C2/c
Zn_4Dy_{11} (**2**)	This work	Dy	**4-**	9	8	1.157	5.599	15	**0.393**	C2/c

Magnetic studies. The magnetic properties for both compounds were measured on a fresh filtered sample of $[Zn_4Ln_{11}]\cdot 19MeOH$, in order to avoid solvent loss. The magnetic susceptibility was recorded between 1.9 and 300 K under an applied field of 1000 Oe (Figure 4). The $\chi_M T$ value of 78.2 cm^3K/mol at 300 K for $[Zn_4Gd_{11}]\cdot 19MeOH$ is smaller than the expected value of 86.7 cm^3K/mol for eleven non-interacting Gd^{III} ions (S = 7/2, $^8S_{7/2}$, g = 2, C = 7.88 cm^3K/mol). On lowering the temperature, the $\chi_M T$ product stays almost constant until 100 K, below which it steadily decreases until it reaches a minimum value of 75.8 cm^3K/mol at 14.0 K. Below 4.7 K further cooling results in the $\chi_M T$ value increasing sharply to reach a value of 79.4 cm^3K/mol at 1.8 K, indicating an onset of dominant ferromagnetic interactions among the lanthanide centers within the complex. The sharp increase in the $\chi_M T$ product can also originate from competing antiferromagnetic interactions within the Ln^{III} centers. This will be further discussed below.

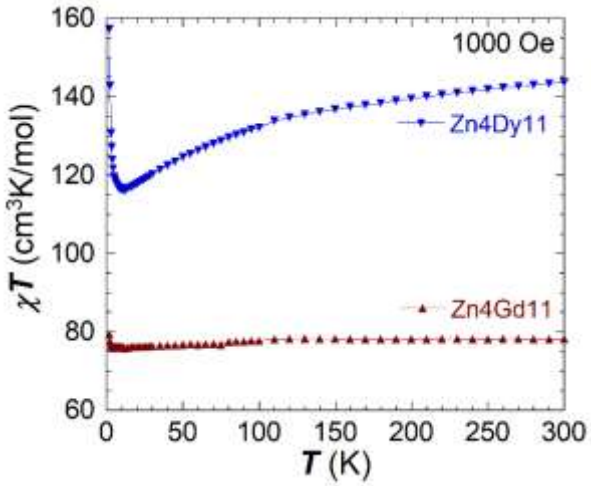

Figure 4. Temperature dependence of the $\chi_M T$ product at 1000 Oe for complex Zn_4Gd_{11} (**1**) (burgundy) and Zn_4Dy_{11} (**2**) (blue).

In the case of $[Zn_4Dy_{11}]\cdot 19MeOH$ the $\chi_M T$ value at 300 K of 143.6 cm^3K/mol is also smaller than the expected value of 155.8 cm^3K/mol for eleven non-interacting Dy^{III} ions (S = 5/2, $^6H_{15/2}$, g = 4/3, C = 14.17 cm^3K/mol). On lowering the temperature, the $\chi_M T$ value steadily decreases until it reaches a minimum value of 115.9 cm^3K/mol at 12.5 K and then steeply increases upon further cooling to

reach a value of 157.2 cm^3K/mol at 1.8 K, which again suggests the presence of intramolecular ferromagnetic interactions or competing antiferromagnetic interactions. This is in contrast to other "diabolo" shaped Gd_9 or Dy_9 cores reported in the literature, which are found to be antiferromagnetically coupled.[14,16,32,41] We believe this is the result of the presence of the tetranuclear $[ZnLn_2Zn(HL2)_2(\mu_2\text{-}MeO)_3Cl_2(MeOH)_2]^{3+}$ "handlebar" unit (Figure 3), containing a dimeric triply-oxygen bridged Ln^{III} motif and the chiral HL2 ligand, with the C_2 axis lying between the two lanthanide metal centers.

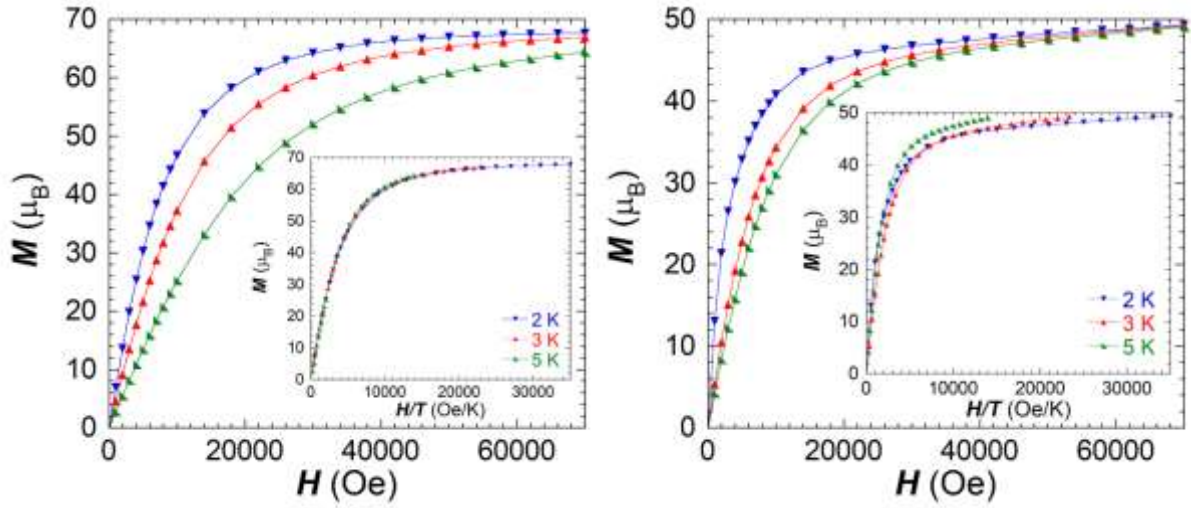

Figure 5. Field dependence of the magnetization plot of $[Zn_4Gd_{11}]\cdot 19MeOH$ (**1**) (left) and $[Zn_4Dy_{11}]\cdot 19MeOH$ (**2**) (right) measured between 0 and 7 T at different temperatures; inset: reduced magnetization.

The field dependence of the magnetization (see Figure 5) was measured between 2.0 to 5.0 K. For $[Zn_4Dy_{11}]\cdot 19MeOH$ (**2**) the lack of saturation in the magnetization values indicates the presence of magnetic anisotropy and/or low-lying excited states. The magnetization curve for compound **2** shows no saturation up to 7.0 T and the values of the isotherms rapidly increase at small fields before following a more gradual linear increase above 1.0 T without saturation. The reduced magnetization plot shown as M vs. H/T as insets in Figure 5, shows the magnetization isotherms which clearly do not superpose onto a single master curve, which indicates the presence of anisotropy within the system. On the other hand, for $[Zn_4Gd_{11}]\cdot 19MeOH$ (**1**), containing the isotropic Gd^{III} ions, the

magnetization shows a rapid increase at small magnetic fields, which also follows a more gradual slope after 1.0 T, and reaches a clear saturation above 4.0 T. The reduced magnetization (Figure 5, inset) shows a superposition of the three isotherms onto one master curve, as expected for an isotropic system. The saturation value of 67.6 μ_B at 7.0 T and 2.0 K is lower than the expected value of 77.0 μ_B for eleven Gd^{III} ions, which are uncoupled or completely ferromagnetically coupled, suggesting that not all metal centers have the same spin orientation.

AC magnetic susceptibility measurements were performed on $[Zn_4Dy_{11}]\cdot 19MeOH$ (**2**) to explore the presence of any slow relaxation of the magnetization compatible with SMM behavior. The frequency-dependent ac susceptibility was measured using various applied fields in attempts to suppress any quantum tunneling of the magnetization (Figure 6).

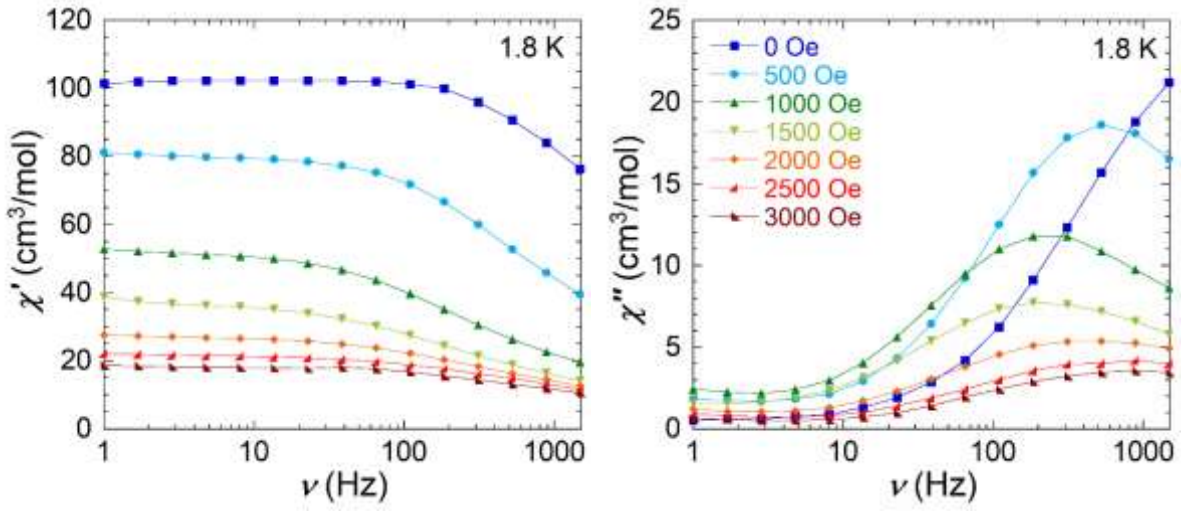

Figure 6. In-phase (left) and out-of-phase susceptibility (right) of $[Zn_4Dy_{11}]\cdot 19MeOH$ (**2**) at varying field at 1.8 K.

Although a frequency-dependent signal is observed without the application of an external field at 1.8 K (Figure 6), the maximum in the out-of-phase signal is not within the measurable frequency range. Since the maxima are shifting by applying a small external field, this indicates that there are additional relaxation processes such as quantum tunneling (QTM) happening. In order to suppress QTM the ac-susceptibility was measured under the optimum applied field of 1000 Oe, where the QTM was found to be smallest (see Figure 6). The ac measurements were carried out under this field

and the data obtained are shown as frequency-dependent in-phase and out-of phase signals in Figure 7 in a temperature range between 1.8 and 4.0 K. In addition, the temperature dependent ac signals are shown in Figure S2, ESI. which show frequency- and temperature-dependent signals with shifting maxima clearly visible. The relaxation time as a function of the temperature (Figure S3, ESI) was analyzed in terms of a ln(τ) versus 1/T plot and fitted to an Arrhenius law to give U_{eff} = 4.4 K and τ_0 = $5.2 \cdot 10^{-5}$ s (R = 0.99). The clear magnetic interactions observed within the Zn_4Gd_{11} complex **1**, suggest that the slow relaxation of magnetization in the case of complex **2** at low temperatures can be attributed to the interplay between the anisotropic Dy^{III} centers within this complex rather than single-ion magnetic behavior.

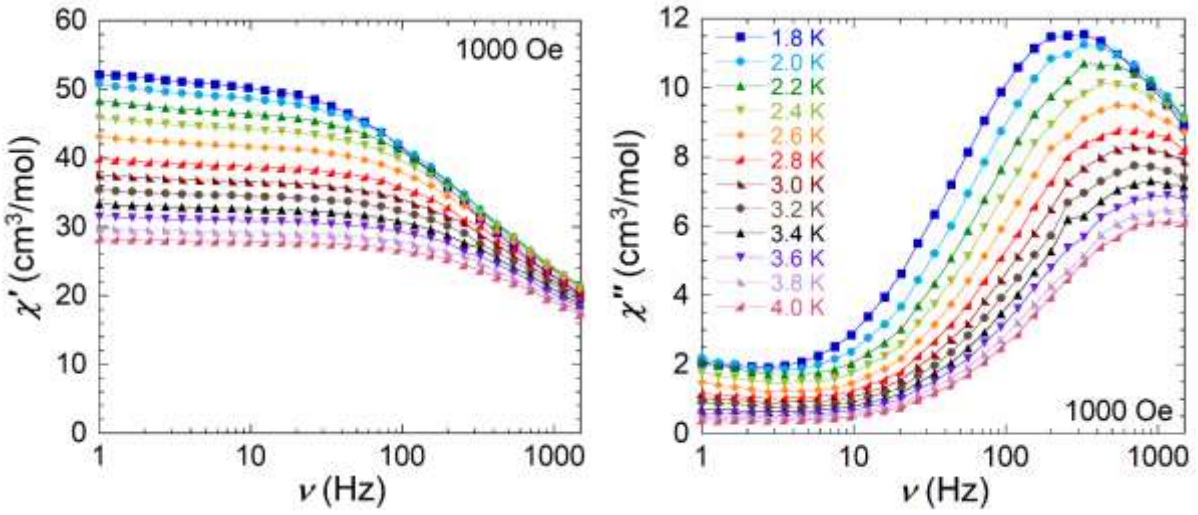

Figure 7. Frequency dependence of the in-phase χ'_M (left) and out-of phase χ''_M (right) susceptibility for $[Zn_4Dy_{11}]\cdot 19MeOH$ (**2**) at different temperatures under an applied field of 1000 Oe.

On its own, the Ln_9 diabolo spin structure is ambiguous as we discuss here for the Gd_9 spin structure. The spins on the squares forming the sandwiching motifs providing the square antiprismatic coordination environment of the central Ln^{III} ion lead to two limiting cases. The known Ln_9 diabolo structures tend towards the first case where the overall contribution of the two sandwich slices is effectively a zero giant spin as a result of antiparallel arrangements of the eight Gd^{III} ions which each provides a 7/2 spin. In this case, the central spin is frustrated and possibly takes an overall average position essentially at right angles to the antiprismatic sandwiching squares. This leads to an

observable but small S = 7/2 spin. In the second limiting case, all the spins would be aligned parallel, which for 9 x Gd^{III} would mean an expected spin ground state of S = 63/2. Neither limiting case has ever been identified, so the question is, why? The compounds we describe here could well provide the answer to this.

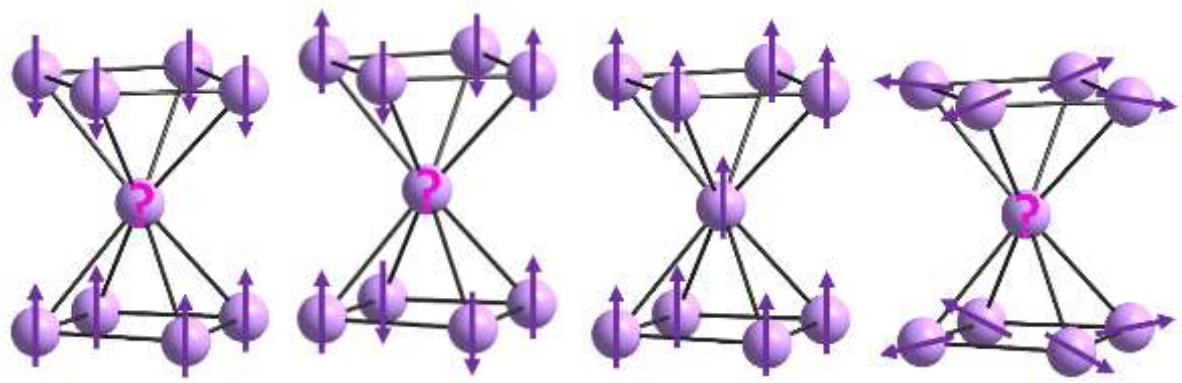

Figure 8. Antiferromagnetic between the Ln_4 squares (**A**), antiferromagnetic within the Ln_4 squares (**B**) ferromagnetic (**C**) and toroidal spin structure (**D**).

For case one (Figure 8 **A**&**B**) we assume 8 antiparallel aligned spins are supplied by the sandwiching parts and thus a contribution of S = 0. So what should the central spin number 9 do? It is essentially frustrated. In case two (Figure 8 **C**) where the spins on the sandwiching part are all parallel the contribution is S = 8 x 7/2 = 56/2 and one might expect the central spin to be parallel to these (S = 63/2). We tend towards case two here in the central diabolo. However, a key feature of the structure is that the introduction of the zinc "feet and hands" along with the tethering rope provided by the connecting Ln ions emphasizes the importance of the C2 symmetry for the diabolo motif. The tethering rope provides a means for directing the spin on the central Ln of the diabolo unit and neatly explains why the spin structure for such units has always seemed ambiguous. Simply put, the central spin does not know which way to turn and is therefore frustrated in the absence of any external influence. Here we can see that through the twisting action provided by the C_2 axis and emphasized by the handlebar motif, the resolution of the inherent chirality into "left or right" explains the induced spin ambiguity of the central Ln of the diabolo.

We used the electrostatically based modelling of Magellan[42] fitting procedure to estimate the orientations of the magnetic anisotropy. The Magellan program is a useful and rather accurate tool for mononuclear lanthanide compounds, but has not been used in multinuclear complexes yet, since magnetic interactions are not included in the calculations. Layfield et al., though, showed for a dimeric Dy complex, that using the Magellan approach provided results similar to those obtained from *ab initio* calculations.[43] Since the Zn^{II} ions are diamagnetic, the magnetic behavior originates solely from the Dy^{III} ions. *Ab initio* calculations on molecules containing more than four metal centers would be incredibly time-consuming considering the vast Hilbert space, while the Magellan approach is a rather fast procedure. Although we cannot know whether the Dy^{III} ions exhibit an Ising-like nature, the fact that they have square-antiprismatic coordination geometries is in line with an Ising ground state,[35] which is conditional for the Magellan approach.

This analysis provides insights into the interplay of the additional Zn_2Dy_2 handle-bar with the Dy_9 diabolo motif. The results of the analysis are shown in Figure 9 and indicate that the magnetic moments are oriented toroidally within the squares of the diabolo motif (Figure 8 **D**), pointing each towards their coordinating nitrate anion on the outside and the μ_4-O^{2-} link in the middle of the metal plane. The axes lie at an angle of 37° to the plane defined by the four Dy^{III} ions (Dy2 to Dy5 and symmetry equivalents).

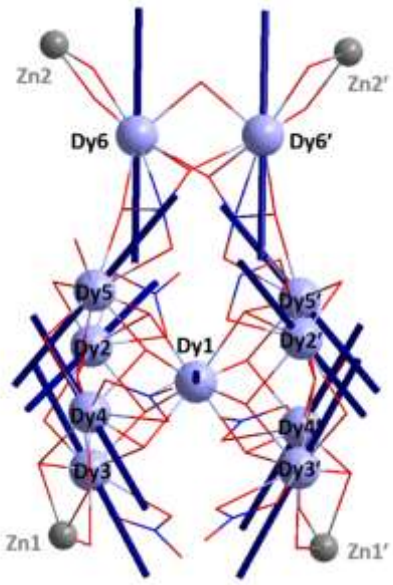

Figure 9. Orientation of the magnetic moments of the ground doublet according to an electrostatic model using the Magellan program, shown as dark blue lines for complex **2**. In this orientation, the uppermost pairs of Zn/Ln ions can be pictured as the hands (Zn) and handles to the (imaginary) rope which will twist the central Ln_9 diabolo in a left or right handed sense whilst the bottom pair of Zn ions can be imagined as the feet of the diabolo artist.

In this case, the Magellan analysis suggests that the constriction at the center of the diabolo corresponding to Dy1, has an orientation where its magnetic anisotropy axis points towards the *a* axis of the crystal system and is thus displaced from the central position of the axially elongated square antiprism sandwiching this central Dy1 ion. The magnetic anisotropy axes of the Dy6 and Dy6' ions are perpendicular to this and thus point towards the *b* axis of the crystal system. This distorted orientation of the magnetic anisotropy axes provides an explanation as to why the magnetization values at 7.0 T and 2.0 K are ca 1/3 smaller than the value expected for eleven Ln^{III} ions, which are either uncoupled or ferro-magnetically coupled.

If we consider the alternative description of the central hourglass as a diabolo, we can find a useful description in terms the role of the outer Dy and Zn (Dy6 and Zn2 and symmetry equivalent) ions. When playing with a diabolo a two handled rope, the $ZnLn_2Zn$ unit, provides a spin direction through the center of the diabolo, here Dy(1), and the performance of the diabolo depends on the applied spin direction induced on the central ion by either a slightly stronger left-hand or right-hand pull on the rope. This inherent induced chirality is clarified on examining the fine details of the molecular structure. Just as in the case of chiral bisphenoid and analogous structures, the scissor angle is crucial in deciding the degree to which the natural chirality of two homochiral scissor blades allows or blocks a cutting action. In the case here we conclude that the distorted orientation of the magnetic anisotropy axes can explain the ambiguity in the orientation of the spin of the central "bottleneck" Dy(1) center of the "diabolo" motif.

CONCLUSIONS

In conclusion, we have produced a system containing the nonanuclear "diabolo" motif, well-known in 4f coordination cluster chemistry, but always with an ambiguous spin structure. By giving this unit "hands and feet" and providing a tethering unit which can direct the spin of the central ion of the diabolo unit we have finally been able to disentangle the "devil in the details" directing the spin structure of such diabolo units.

Acknowledgements

We thank the EPSRC (UK) for funding (grant number EP/M023834/1) and the EPSRC UK National Crystallography Service at the University of Southampton[23] for the collection of the crystallographic data for compounds **1** and **2**. IAK and AKP acknowledge DFG (SFB/TRR 88 – 3MET) and the Helmholtz Gemeinschaft POF STN for funding. We thank Dr. Yan Peng for collecting some magnetic data. IAK thanks the Irish Research Council (IRC) for the GOIPD/2016/503 fellowship.

Conflict of Interest Disclosure.

The authors declare no competing financial interest.

Corresponding Author

G.Kostakis@sussex.ac.uk, annie.powell@kit.edu

Funding Sources

EP/M023834/1

SFB/TRR 88 – 3MET

Supporting Information.

Crystal structures (cif files), thermogravimetric analysis (TGA) of compound **1** (Fig S1), magnetic data.

References

(1) Chen, W.-P.; Liao, P.-Q.; Yu, Y.; Zheng, Z.; Chen, X.-M.; Zheng, Y.-Z. A Mixed-Ligand Approach for a Gigantic and Hollow Heterometallic Cage {Ni 64 RE 96 } for Gas Separation

and Magnetic Cooling Applications. *Angew. Chem. Int. Ed.* **2016**, *55*, 9375–9379.

(2) Griffiths, K.; Kostakis, G. E. Transformative 3d-4f Coordination Cluster Carriers. *Dalton. Trans.* **2018**, *47*, 12011–12034.

(3) Moreno Pineda, E.; Chilton, N. F.; Tuna, F.; Winpenny, R. E. P.; McInnes, E. J. L. Systematic Study of a Family of Butterfly-Like {M<inf>2</Inf>Ln<inf>2</Inf>} Molecular Magnets (M = Mg^{II}, Mn^{III}, Co^{II}, Ni^{II}, and Cu^{II}; Ln = Y^{III}, Gd^{III}, Tb^{III}, Dy<sup>. *Inorg. Chem.* **2015**, *54*, 5930–5941.

(4) Mondal, K. C.; Sundt, A.; Lan, Y.; Kostakis, G. E.; Waldmann, O.; Ungur, L.; Chibotaru, L. F.; Anson, C. E.; Powell, A. K. Coexistence of Distinct Single-Ion and Exchange-Based Mechanisms for Blocking of Magnetization in a Co II 2Dy III 2 Single-Molecule Magnet. *Angew. Chemie - Int. Ed.* **2012**, *51*, 7550–7554.

(5) Mondal, K. C.; Kostakis, G. E.; Lan, Y.; Wernsdorfer, W.; Anson, C. E.; Powell, A. K. Defect-Dicubane Ni2Ln2 (Ln = Dy, Tb) Single Molecule Magnets. *Inorg. Chem.* **2011**, *50*, 11604–11611.

(6) Peng, G.; Kostakis, G. E.; Lan, Y.; Powell, A. K. Body-Wing Swapping in Butterfly {Fe(III)2Ln(III)2} Coordination Clusters with Triethylene Glycol as Ligand. *Dalton Trans.* **2013**, *42*, 46–49.

(7) Langley, S. K.; Chilton, N. F.; Ungur, L.; Moubaraki, B.; Chibotaru, L. F.; Murray, K. S. Heterometallic Tetranuclear [Ln(III)2Co(III)2] Complexes Including Suppression of Quantum Tunneling of Magnetization in the [Dy(III)2Co(III)2] Single Molecule Magnet. *Inorg. Chem.* **2012**, *51*, 11873–11881.

(8) Baniodeh, A.; Magnani, N.; Lan, Y.; Buth, G.; Anson, C. E.; Richter, J.; Affronte, M.; Schnack, J.; Powell, A. K. High Spin Cycles: Topping the Spin Record for a Single Molecule Verging on Quantum Criticality. *npj Quantum Mater.* **2018**, *3*, 10.

(9) Kostakis, G. E.; Blatov, V. A.; Proserpio, D. M. A Method for Topological Analysis of High Nuclearity Coordination Clusters and Its Application to Mn Coordination Compounds. *Dalton*

Trans. **2012**, *41*, 4634–4640.

(10) Papaefstathiou, G. S.; Escuer, A.; Vicente, R.; Font-Bardia, M.; Solans, X.; Perlepes, S. P. Reactivity in Polynuclear Transition Metal Chemistry as a Means to Obtain High-Spin Molecules: Substitution of Mu(4)-OH- by Eta 1,Mu(4)-N-3(-) Increases Nine Times the Ground-State S Value of a Nonanuclear Nickel(II) Cage. *Chem. Commun.* **2001**, 2414–2415.

(11) Papaefstathiou, G. S.; Raptopoulou, C. P.; Tsohos, A.; Terzis, A.; Bakalbassis, E. G.; Perlepes, S. P. Alcoholysis of 2,2'-Pyridil, (2-C5H4N)C(O)C(O)(2-C5H4N), Iin the Presence of Copper(II): A Family of Planar Pentanuclear Copper(II) Complexes Stabilized by [(2-C5H4N)C(O)(OR)C(O)(OR)(2-C5H4N)]2- and Carboxylate Ligands. *Inorg. Chem.* **2000**, *39*, 4658–4662.

(12) Xu, X.; Zhao, L.; Xu, G.-F.; Guo, Y.-N.; Tang, J.; Liu, Z. A Diabolo-Shaped Dy9 Cluster: Synthesis, Crystal Structure and Magnetic Properties. *Dalton Trans.* **2011**, *40*, 6440–6444.

(13) Zheng, S.-R.; Chen, R.-L.; Xie, T.; Liu, Z.-M.; Wen, X.-L.; Chen, X.-Y.; Fan, J.; Zhang, W.-G. Construction of Several New S-/p-Block Complexes Containing Binuclear Metal-Terpyridine Building Blocks: Dependence of Structural Diversity on the Number of Coordinated Water Molecules. *CrystEngComm* **2014**, *16*, 4029–4037.

(14) Xu, G.; Wang, Z.; He, Z.; Zhi, L.; Liao, C.; Yan, C.; Lu, Z. Synthesis and Structural Characterization of Nonanuclear Lanthanide Complexes Synthesis and Structural Characterization of Nonanuclear Lanthanide Complexes. *Inorg. Chem.* **2002**, *41*, 6802–6807.

(15) Petit, S.; Baril-Robert, F.; Pilet, G.; Reber, C.; Luneau, D. Luminescence Spectroscopy of Europium(III) and Terbium(III) Penta-, Octa- and Nonanuclear Clusters with Beta-Diketonate Ligands. *Dalton Trans.* **2009**, 6809–6815.

(16) Alexandropoulos, D. I.; Mukherjee, S.; Papatriantafyllopoulou, C.; Raptopoulou, C. P.; Psycharis, V.; Bekiari, V.; Christou, G.; Stamatatos, T. C. A New Family of Nonanuclear Lanthanide Clusters Displaying Magnetic and Optical Properties. *Inorg. Chem.* **2011**, *50*, 11276–11278.

(17) Gamer, M. T.; Lan, Y.; Roesky, P. W.; Powell, A. K.; Clerac, R. Pentanuclear Dysprosium Hydroxy Cluster Showing Single-Molecule-Magnet Behavior. *Inorg. Chem.* **2008**, *47*, 6581–6583.

(18) Kloewer, F.; Lan, Y.; Nehrkorn, J.; Waldmann, O.; Anson, C. E.; Powell, A. K. Modelling the Magnetic Behaviour of Square-Pyramidal Co-5(II) Aggregates: Tuning SMM Behaviour through Variations in the Ligand Shell. *Chem. Eur. J.* **2009**, *15*, 7413–7422.

(19) Griffiths, K.; Kumar, P.; Akien, G. R.; Chilton, N. F.; Abdul-Sada, A.; Tizzard, G. J.; Coles, S. J.; Kostakis, G. E. Tetranuclear Zn/4f Coordination Clusters as Highly Efficient Catalysts for Friedel–Crafts Alkylation. *Chem. Commun.* **2016**, *52*, 7866–7869.

(20) Trivedi, E. R.; Eliseeva, S. V.; Jankolovits, J.; Olmstead, M. M.; Petoud, S.; Pecoraro, V. L. Highly Emitting Near-Infrared Lanthanide "Encapsulated Sandwich" Metallacrown Complexes with Excitation Shifted toward Lower Energy. *J. Am. Chem. Soc.* **2014**, *136*, 1526–1534.

(21) Stavgianoudaki, N.; Siczek, M.; Lis, T.; Inglis, R.; Milios, C. J. A Triacontanuclear [Zn 12 Dy 18] Cluster: A Ring of [Dy 4] Cubes. *Chem. Commun.* **2016**, *52*, 343–345.

(22) Zhang, L.; Zhao, L.; Zhang, P.; Wang, C.; Yuan, S.-W.; Tang, J. Nanoscale {Ln(III)24Zn(II)6} Triangular Metalloring with Magnetic Refrigerant, Slow Magnetic Relaxation, and Fluorescent Properties. *Inorg. Chem.* **2015**, *54*, 11535–11541.

(23) Coles, S. J.; Gale, P. A. Changing and Challenging Times for Service Crystallography. *Chem. Sci.* **2012**, *3*, 683–689.

(24) Sheldrick, G. M. Crystal Structure Refinement with SHELXL. *Acta Crystallogr. Sect. C Struct. Chem.* **2015**, *71*, 3–8.

(25) Spek, A. L. Single-Crystal Structure Validation with the Program PLATON. *J. Appl. Crystallogr.* **2003**, *36*, 7–13.

(26) Dolomanov, O. V.; Bourhis, L. J.; Gildea, R. J.; Howard, J. A. K.; Puschmann, H. OLEX2 : A Complete Structure Solution, Refinement and Analysis Program. *J. Appl. Crystallogr.* **2009**,

42, 339–341.

(27) Farrugia, L. J. WinGX and ORTEP for Windows : An Update. *J. Appl. Crystallogr.* **2012**, *45*, 849–854.

(28) Macrae, C. F.; Edgington, P. R.; McCabe, P.; Pidcock, E.; Shields, G. P.; Taylor, R.; Towler, M.; Van De Streek, J. Mercury: Visualization and Analysis of Crystal Structures. *J. Appl. Crystallogr.* **2006**, *39*, 453–457.

(29) Darensbourg, D. J.; Karroonnirun, O.; Wilson, S. J. Ring-Opening Polymerization of Cyclic Esters and Trimethylene Carbonate Catalyzed by Aluminum Half-Salen Complexes. *Inorg. Chem.* **2011**, *50*, 6775–6787.

(30) Xu, X.-Y.; Chen, Q.-C.; Yu, Y.-D.; Huang, X.-C. Ligand Induced Anionic Cuprous Cyanide Framework for Cupric Ion Turn on Luminescence Sensing and Photocatalytic Degradation of Organic Dyes. *Inorg. Chem.* **2016**, *55*, 75–82.

(31) Zou, H. H.; Sheng, L. B.; Chen, Z. L.; Liang, F. P. Lanthanide Nonanuclear Clusters with Sandglass-like Topology and the SMM Behavior of Dysprosium Analogue. *Polyhedron* **2015**, *88*, 110–115.

(32) Singh-Wilmot, M. A.; Sinclair, R. A.; Andrews, M.; Rowland, C.; Cahill, C. L.; Murugesu, M. Nonanuclear Lanthanide(III) Nanoclusters: Structure, Luminescence and Magnetic Properties. *Polyhedron* **2013**, *53*, 187–192.

(33) Omagari, S.; Nakanishi, T.; Kitagawa, Y.; Seki, T.; Fushimi, K.; Ito, H.; Meijerink, A.; Hasegawa, Y. Critical Role of Energy Transfer Between Terbium Ions for Suppression of Back Energy Transfer in Nonanuclear Terbium Clusters. *Sci. Rep.* **2016**, *6*, 37008.

(34) Sorace, L.; Benelli, C.; Gatteschi, D. Lanthanides in Molecular Magnetism: Old Tools in a New Field. *Chem. Soc. Rev.* **2011**, *40*, 3092–3104.

(35) Rinehart, J. D.; Long, J. R. Exploiting Single-Ion Anisotropy in the Design of f-Element Single-Molecule Magnets. *Chem. Sci.* **2011**, *2*, 2078–2085.

(36) Feltham, H. L. C.; Brooker, S. Review of Purely 4f and Mixed-Metal Nd-4f Single-Molecule

Magnets Containing Only One Lanthanide Ion. *Coord. Chem. Rev.* **2014**, *276*, 1–33.

(37) M. Llunell, D. Casanova, J. Cirera, P. Alemany, S. A. SHAPE. *SHAPE version 2.0.* **2010**, *Barcelona*.

(38) Addison, A. W.; Rao, T. N.; Reedijk, J.; Vanrijn, J.; Verschoor, G. C. Synthesis, Structure and Spectroscopic Properties of Copper(II) Compounds Containing Nitrogen Sulphur Ligands – The Crystal and Molecular Structure of Aqua 1,7-Bis(n-Methylbenzimidazol-2'-Yl)-2,6-Dithiaheptane Copper(II) Perchlorate. *J. Chem. Soc. Trans.* **1984**, 1349–1356.

(39) Zhou, Y.-Y.; Geng, B.; Zhang, Z.-W.; Guan, Q.; Lu, J.-L.; Bo, Q.-B. New Family of Octagonal-Prismatic Lanthanide Coordination Cages Assembled from Unique Ln17 Clusters and Simple Cliplike Dicarboxylate Ligands. *Inorg. Chem.* **2016**, *55*, 2037–2047.

(40) Xu, G.; Wang, Z.-M.; He, Z.; Lu, Z.; Liao, C.-S.; Yan, C.-H. Synthesis and Structural Characterization of Nonanuclear Lanthanide Complexes. *Inorg. Chem.* **2002**, *41*, 6802–6807.

(41) Wang, K.; Chen, Z.-L.; Zou, H.-H.; Zhang, Z.; Sun, W.-Y.; Liang, F.-P. Two Types of Cu-Ln Heterometallic Coordination Polymers with 2-Hydroxyisophthalate: Syntheses, Structures, and Magnetic Properties. *Cryst. Growth Des.* **2015**, *15*, 2883–2890.

(42) Chilton, N. F.; Collison, D.; McInnes, E. J. L.; Winpenny, R. E. P.; Soncini, A. An Electrostatic Model for the Determination of Magnetic Anisotropy in Dysprosium Complexes. *Nat. Commun.* **2013**, *4*, 2551.

(43) Day, B. M.; Chilton, N. F.; Layfield, R. Molecular and Electronic Structures of Donor-Functionalized Dysprosium Pentadienyl Complexes. *Dalton Trans.* **2015**, *44*, 7109–7113.

For Table of Contents Only

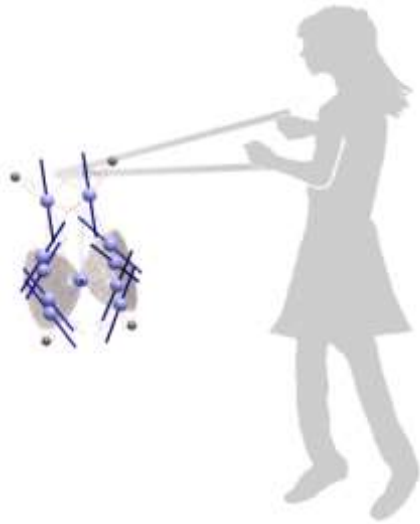

Synopsis

Magnetic studies of Zn_4Ln_{11} [Ln is Gd(**1**), Dy (**2**)] demonstrate the importance of the central spin orientation in the spin structure of the ambiguous Ln_9-diabolo motif.